Ceramics International 51 (2025) 52066–52073

Contents lists available at ScienceDirect

Ceramics International

journal homepage: www.elsevier.com/locate/ceramint

Matrix fracture energy as a function of porosity for all oxide ceramic matrix composites

Lukas Wagner *, Georg Puchas, Stefan Flauder, Bernd Martin, Stefan Schafföner

Chair of Ceramic Materials Engineering (CME), University of Bayreuth, Bayreuth, Germany

ARTICLE INFO

Handling Editor: Dr P. Vincenzini

Keywords:
Porosity
Mechanical testing
Fracture energy
Ceramic matrix composites (CMCs)

ABSTRACT

This study presents an easy way to investigate the suitability of a porous material as a matrix for a weak matrix composite (WMC) according to the model of He and Hutchinson without the use of expensive fibers. The influence of porosity on the fracture energy of a monolithic alumina-zirconia matrix system developed for an all-oxide ceramic matrix composite (Ox/Ox) was used to compare theoretical predictions with the real Ox/Ox behavior', which we presented in our previous study. The Ox/Ox material used for the comparison was a combination of α-alumina Nextel™ 610 fibers embedded in the said alumina-zirconia matrix system. The matrix fracture energy was determined on monolithic samples using a three-point-bending test, based on the work-of-fracture approach. By using the ratio between the determined fracture energy and the fracture energy of dense alumina fibers, it was possible to classify our material in the theoretical model. The results showed, that the method allowed a precise prediction of the damage-tolerant behavior of a CMC, thereby enabling the development of future matrix materials by using solely monolithics.

1. Introduction

The incorporation of ceramic fibers in a ceramic matrix is a very effective method to avoid the brittle fracture behavior of monolithic ceramics. Due to energy dissipating mechanisms such as crack deflection or fiber pull-out, ceramic matrix composites (CMCs) do not exhibit a catastrophic fracture behavior, therefore rendering them more suitable for structural applications than monolithics [1].

To enable this damage-tolerant behavior of CMCs, two different approaches are applied. While weak interface composites (WICs) use a fiber coating to ensure crack deflection at the fiber/matrix interface, weak matrix composites (WMCs) utilize a highly porous matrix [1–3]. Both approaches are based on the theoretical study of He and Hutchinson [4], which described the crack propagation behavior at an interface between materials with different elastic properties. Since CMCs depend on the crack deflection at the fiber-matrix interface, the study played a major role for the conceptual design of CMCs.

$$elastic\ mismatch = \frac{E_f - E_m}{E_f + E_m} \quad (1)$$

In order to achieve crack deflection, it is favorable that the elastic mismatch (equation (1)), i.e. the difference between the Young's moduli of fibers (E_f) and matrix (E_m) divided by their sum, is high and the ratio of the fracture energies of the fiber/matrix-interface and the fiber is low. In this case, a crack will be deflected at the interface, thereby preventing or at least delaying its propagation into the fibers [4]. The concept was further developed in different studies, showing its validity and enabling the development of the general design for WMCs [5–8]. The fracture behavior was also subsequently investigated, leading to the model of H-cracks propagating through the material during fracture [6].

In order to classify an existing CMC within the model of He and Hutchinson, the fracture energies and elastic moduli of the matrix and the interface must be determined. For the WIC concept, it is very difficult to determine the fracture energy of the protective coating, since it can only be determined within a CMC. Hence, the determination has to be carried out with fiber push-in or push-out tests [9]. The same methods can be also applied for WMCs. Nevertheless, it can be argued, that within a WMC, the fracture energy of the interface between the fiber and matrix cannot be higher than the fracture energy of the matrix itself, since the concept solely relies on the porosity and therefore the fracture energy of the matrix [10–12]. In this case, the determination of the fracture energy of the matrix is sufficient to calculate the fracture energy ratio for the classification according to the model of He and Hutchinson [10,13]. In another approach, the K_{IC} and the Young's modulus were estimated

* Corresponding author.
E-mail address: Lukas1.Wagner@uni-bayreuth.de (L. Wagner).

https://doi.org/10.1016/j.ceramint.2025.08.414
Received 4 July 2025; Received in revised form 18 August 2025; Accepted 27 August 2025
Available online 27 August 2025

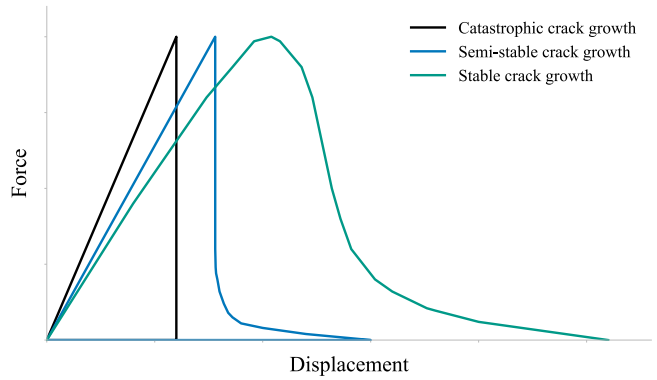

Fig. 1. Schematic force-displacement curves for catastrophic, semi-stable and stable crack growth based on Wang et al. [15]. During the test and before fracture, energy is stored elastically within the system of sample and testing machine. If the stored energy exceeds the energy required for a complete crack, catastrophic crack growth occurs in the moment of failure.

using the porosity-property-relationship of monolithic samples to predict crack deflection of different interfaces [13].

The fracture energy can be calculated based on the work necessary for a stable crack growth in a monolithic sample in relation to the area of the cracked surface. The work of fracture can be therefore determined as the area under the force-displacement curve of a sample with stable or semi-stable crack growth. Consequently, achieving a stable or semi-stable crack growth is essential [14–16]. Schematic force-displacement curves for the three possible states of fracture behavior are displayed in Fig. 1.

The energy during testing and before fracture of the sample can be divided into the elastically stored energy within the sample and the testing setup, which is set free once the crack starts propagating. During a stable or semi-stable crack growth, the amount of stored energy is not sufficient to enable crack growth through the whole sample. As a result, additional energy must be supplied to the system to complete the cracking process. Hence, to achieve a (semi-) stable crack growth, the samples have to be notched to ensure a minimal storage of elastic energy before the crack initiation. If the overall stored elastic energy of the sample and the testing setup surpasses the energy needed for a complete crack growth, catastrophic failure will occur and the determination of the work of fracture is impossible [17].

The work-of-fracture method was used by Fujita et al. in different studies [12,18,19] to predict the influence of thermal aging on the damage-tolerant behavior of potential matrix materials. While the investigation started with the aging of all-oxide CMC (Ox/Ox) [19,20], its focus was mainly on the characterization of matrix materials, without verifying the results on CMC [12,21]. However, none of the variations led to crossing the model line of crack deflection in the He and Hutchinson diagram, although experiments using a deflection parameter introduced in their work indicated the loss of damage-tolerant behavior after a certain amount of infiltrations with a ceramic precursor [21]. However, this prediction of a loss of damage tolerant behavior was not experimentally verified on CMC.

The Ox/Ox material on which this study is based was already discussed in several publications [22–26]. In our recent study, we demonstrated, how the porosity of the matrix affects the crack deflection and therefore the damage-tolerant behavior [26]. Similar investigations were performed in other recent studies [27–29]. The aim of this study is to use our research on the densification of the material as a model system and to provide a method to predict the damage-tolerant behavior (or lack thereof) without using fibers at all. This allows a cost efficient development of new matrix systems for WMC without the influences of fibers, making it a fast and easy to use method for checking the overall suitability of a material. In this regard, the study determines all necessary data such as Young's modulus and fracture energy as a function of the porosity of the material. Since reliable values for the fracture energy are dependent on the used material system and are therefore not readily available [30], this study focuses on the experimental determination of the fracture energy of monolithic samples using the work-of-fracture approach. By describing the procedure in detail, it should enable others to use this simple method for their investigations. In order to achieve full comparability and thereby ensure a reasonable prediction of the behavior of a WMC, this study was performed on monolithic samples with the same composition as the matrix of the Nextel™ 610/Al_2O_3-ZrO_2 – Ox/Ox of our prior study [26]. The predictions were compared to the data of the previous study to validate the method.

2. Experiments an methods

2.1. Matrix concept and materials

The matrix of the all-oxide ceramic matrix composite (Ox/Ox) investigated in our previous study [26] consisted of a mixture of coarse-grained Al_2O_3 (d_{50} = 0.7 µm, CT 3000 SG, Almatis, Germany), fine-grained Al_2O_3 (d_{50} = 0.23 µm [31], TM-DAR, Taimei Chemicals, Japan), and fine tetragonal ZrO_2 (d_{50} = 0.1 µm, TZ-3Y-E, Tosoh Corp., Japan) with a ratio of 70/5/25 by weight. The mixture was developed to meet the requirements of the weak matrix concept, which uses a fine scaled porosity of 30–40 vol% to enable a damage-tolerant behavior in the composite material [1,2,32,33]. The coarse powder provides a non-shrinking network, which is bonded through the sufficient sintering activity of the two fine powders. Due to this composition, a submicron matrix porosity of around 45 % is reached in the composite. The slurry also contained glycerol, water and a dispersant (Sokalan PA 15, BASF, Germany). The solid content was adjusted to 67 wt%. Cast monolithic samples with the same slurry composition were manufactured. They showed a lower porosity of 40.8 % compared to the submicron matrix porosity of the Ox/Ox. The lower porosity of the monolithic matrix is to be expected, as there are no fibers inhibiting the formation of a dense packing of the particles [34].

Sequential densification steps of the matrix were carried out using zirconium-n-butoxide in butanol (Alfa Aesar™ Zirconium-n-butoxide, 80 % (w/w) in 1-Butanol) to infiltrate the open porosity of the monolithic samples and therefore mimicking the treatment used for our Ox/Ox material. This precursor has a high ceramic yield and does not produce acid residues. It provided a good possibility to vary the porosity of the Ox/Ox and was also used to lower the porosity of the samples manufactured in our previous studies [26,32].

2.2. Processing

The samples to determine the Young's modulus and fracture energy were fabricated by slip casting. Since the manufacturing of Ox/Ox takes place without a capillary active mold [22–26], slip casting of the monolithic was carried out in a dense PTFE mold to form samples with 60 mm length, 10 mm thickness and 6 mm width. The samples were dried for 48 h at 30 °C, followed by 24 h at 50 °C to guarantee a crack free green body. After demolding, the final drying took place at 100 °C for at least 12 h. The final height of the samples was adjusted to 5 mm by grinding with a P80 SiC abrasive paper. Afterwards, the green bodies were sintered in air at 1225 °C for 2 h, using the same sintering program as for the Ox/Ox material [22–26]. 270 samples were fabricated in total. In principal, fibers in an Ox/Ox can cause constrained sintering, which as a worst case might lead to a large area fiber/matrix debonding and in turn to a significant decrease in mechanical properties. For Ox/Ox, this is prevented by using non-shrinking matrix systems which only exhibit the occasional segmentation cracks perpendicular to the fabrics but none at the fiber/matrix-interface. The investigated material system has been designed to lead to very little shrinkage and the numerous

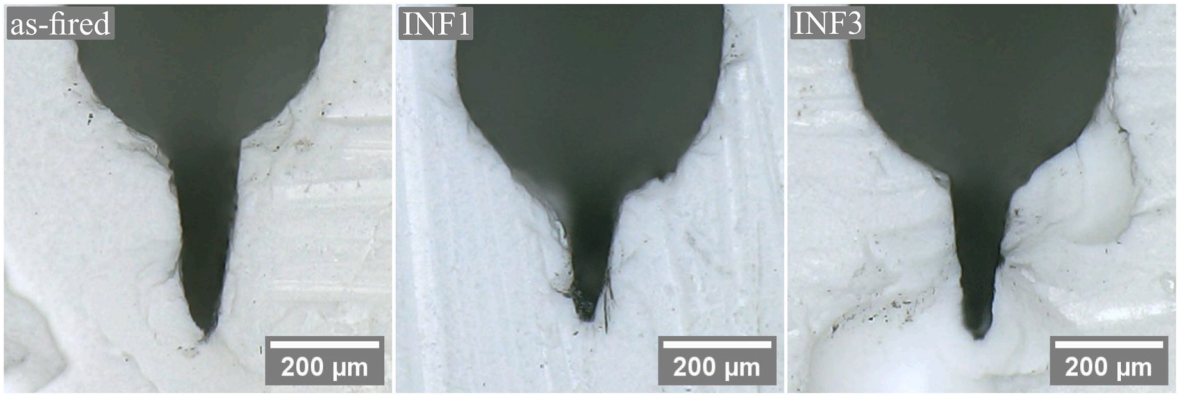

Fig. 2. Optical microscope images of different polished notches. The sawed tip can be seen as the big radius at the upper edge, i.e. where the polished crack tip emerges from. The notch tip had a radius of 30 ± 5 µm.

publications on the system have shown that it enables good mechanical properties [22–26]. The shrinkage of the matrix is therefore minimal, which is why no major changes in the microstructure or crack pattern of the monolithic samples compared to Ox/Ox were expected. Since particles can arrange freely in the monolithic samples, a minor change in porosity was expected, especially due to the fact, that the porosity at a fiber/matrix interface is always increased in comparison to the matrix itself [34].

After the initial sintering, the samples were randomly separated in nine groups with 30 samples for each group. The "as-fired" samples served as an overall reference and underwent no further treatment. The "heat-treated" samples underwent all subsequent heat treatments necessary to convert the precursor to ZrO_2, but were not infiltrated to investigate possible effects of the heat treatments on the material properties.

To ensure comparability, the infiltration procedure was the same as the one used in our previous work to vary the porosity of an Ox/Ox [26]. The samples were evacuated for 1 h in a desiccator, followed by the filling of the precursor into the desiccator using a valve until all samples were submerged. The samples remained in vacuum (<20 mbar) for at least 2 h before atmospheric pressure was restored and the samples were removed from the precursor bath. After hydrolyzing for 12 h at ambient conditions, the conversion of the precursor took place during a heat treatment for 2 h at 950 °C in air. Since the procedure was repeated up to seven times, the samples are referred to as "INF1"–"INF7". The final heat treatment was carried out for 2 h at 1225 °C in order to crystallize the precursor. All infiltrated samples underwent the complete heat treatment cycle, i.e. six times 2 h at 950 °C and a single treatment of 2 h at 1225 °C.

2.3. Characterization

The apparent porosity was determined by water immersion (Archimedes' principle) according to DIN EN 1389. For the investigation of the microstructure, representative samples were embedded in resin, ground and polished. Afterwards, the resin was burned out for 2 h at 700 °C in air in order to enable the analysis of the submicron porosity. The polished microstructure was investigated by scanning electron microscopy (SEM, Sigma 300 VP, Zeiss, Germany).

After sintering, the dynamic Young's modulus was determined using the impulse excitation technique (IET, MK7 Advanced, GrindoSonic, Belgium) according to ASTM E 1876-01.

To prepare the samples for fracture energy testing, a notch was cut into the center of every sample using a diamond wire saw (Type 6234, Well, Germany) with a 0.5 mm wire diameter and a diamond size of 64 µm. The notch depth was 0.6 times the sample thickness, i.e. 6 mm. Afterwards, the notch was polished by hand with 3 µm diamond suspension (DP-Suspension P 3 µm, Struers, Denmark) and a razor blade in accordance to DIN EN ISO 23146. After polishing, the notch diameter was determined using a digital optical microscope (DSX 1000, Olympus, Japan). Fig. 2 shows optical microscope images of three different polished notches, which are representative for all samples, as examples for the notch geometry.

The radius of the notch tip was 30 ± 5 µm for all samples, while the mean notch depth was 290 ± 45 µm. Both, the radius of the tip as well as the notch depth, were determined on at least 50 different samples, randomly distributed over all sample types.

The fracture energy was investigated by a work-of-fracture three-point-bending test [15,17,35]. A schematic representation of the setup can be seen in Fig. 3. Compared to the standard mentioned above (DIN EN ISO 23146), a bigger sample size of 60 × 10 × 6 mm^3 compared to the standard size of 35 × 4 × 3 mm was used, since the standard does not mention (semi-) stable crack growth. The bigger sample size was therefore inspired by the work-of-fracture tests described in literature to meet the required support span-to-width ratio of four, commonly used for this test [14,15]. Therefore, the lower support span was set to 40 mm. Additionally, a lower testing speed of 0.005 mm/min compared to the literature [14] was used to ensure a stable or semi-stable fracture behavior. The testing machine (Z050 TEW AllroundLine, ZwickRoell, Austria) was equipped with a 5 kN force measuring cell to detect the force *P*, since it enables a good machine stiffness and sufficient precision. The displacement υ was recorded with a video extensometer. The crack surface area *A* was investigated using optical microscope images of the fracture surface and the software ImageJ (National Institutes of Health, USA). The fracture energy was calculated using equation (2), with v_c being the displacement at complete fracture [36].

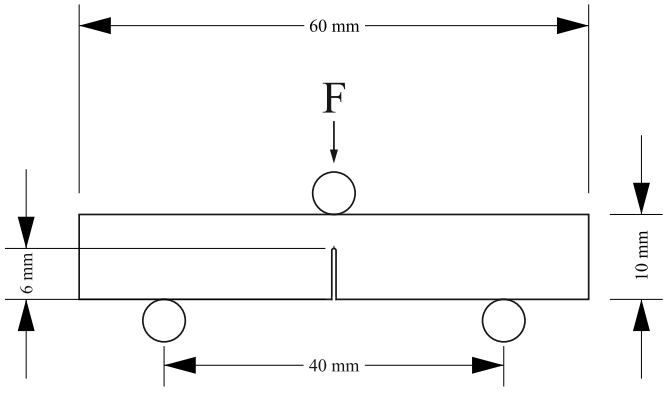

Fig. 3. Schematic representation of the sample size and the setup used in the adapted work-of-fracture test.

$$\textit{fracture energy} = \frac{\int_0^{v_c} P\, dv}{A} \quad (2)$$

The maximum force of the test was also used to determine the fracture toughness K_{1c} in accordance with DIN EN ISO 23146 for notched three-point-bending tests. Despite the fact that the test specimens were bigger than mentioned in the standard, the method still enables an approximation of K_{1c}.

3. Results and discussion

3.1. Influence of decreased porosity on mechanical properties

3.1.1. Porosity decrease

The conversion behavior of the precursor was investigated in our previous study, for detailed information please refer to Wagner et al. [26]. According to the manufacturer, a theoretical ZrO_2 yield of 26 wt% to 29 wt% is possible, which was confirmed by a thermogravimetric measurement (not shown). The conversion of the precursor took place until 400 °C, but preliminary tests showed carbon residues after a heat treatment at 600 °C. Therefore, the heat treatment was carried out at 950 °C to ensure a complete conversion of the precursor as well as a full oxidation of the carbon residues. To ensure a comparable infiltration, all samples were infiltrated using the same precursor batch.

To faciliate a comparison to our previous work [26], the infiltration steps as well as the heat treatments for the monolithic samples were carried out in the same way as for the Ox/Ox material. Starting with an initial porosity of 40.8 %, the porosity was reduced gradually up to four infiltrations. However, five to seven infiltrations were not able to densify the samples further, instead a porosity plateau was reached at about 34.5 %, as can be seen in Fig. 4. Confidence intervals are displayed in Fig. 4, hence the samples with more than four infiltrations show the same porosity. Additionally, there was no difference in porosity between as-fired and heat-treated samples. The results are in agreement with that of the Ox/Ox investigated in our previous study. Since fibers essentially disrupt the powder packing and therefore lead to a higher porosity than in a comparable monolithic material, the fiber-reinforced material of our previous study had an initial submicron matrix porosity of 46.4 % in the as-manufactured state [26]. For the same reason, the fracture energy of the matrix will always exceed that of the fiber/matrix interface. Since the damage-tolerant behavior of the composite material benefits from a higher porosity (i.e. lower fracture energy), the prediction based on the matrix values will tend to underestimate the potential for crack deflection of the actual composite.

The plateau suggests that the repeated infiltrations create a porosity gradient from the outside to the inside, which prevents further precursor penetration into the sample. However, this gradient was not observed in SEM images. Since the aim of the study was to investigate a simple method for determination of the fracture energy and to compare the predictions enabled by these experiments with the findings in the Ox/Ox material, the gradient was not investigated further. Nevertheless, it may have an influence on the obtained results and should be considered in the development of new materials.

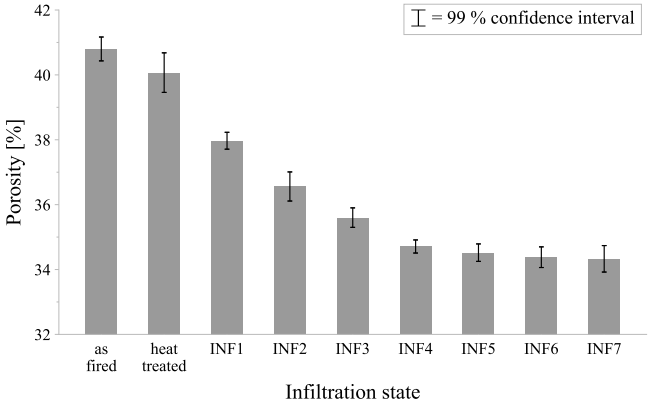

Fig. 4. Mean porosity of all nine sample types. After four infiltrations, a porosity plateau was reached, resulting in a similar porosity of around 34.5 %. The error bars show the confidence interval for 99 % with a sample size of 30 for each batch.

3.1.2. Influence of the heat treatment

Each infiltration cycle requires a separate heat treatment for the conversion of the precursor. Therefore, infiltrated samples are exposed to high temperatures for a significantly longer period of time than as-fired samples. This may influence the measured properties of the samples. In order to investigate this possible influence, samples with and without heat treatments were compared regarding the fracture energy and Young's modulus. In Fig. 5 the fracture energy and the Young's modulus of "heat-treated" as well as of "as-fired" samples are marked with circles for better comparison. The error bars show the 99 % confidence interval of the samples. This indicates that the heat treatments did not influence the fracture energy of the samples. In addition, the fracture toughness remains the same (0.54 MPa•$m^{0.5}$ and 0.53 MPa•$m^{0.5}$). While the microstructural investigations of polished samples did not indicate an influence of the heat treatment, i.e. no microstructural changes, the Young's modulus increased slightly after heat treatment from 46 GPa to 51 GPa (Fig. 5, data in blue). This might be caused by the slight decrease of porosity measured for the heat-treated samples (40.8 % vs 40.0 %), which is due to some densification enabled by the heat treatments. Therefore, the heat treatment of the samples lowers the elastic mismatch in the classification of the matrix material, but the fracture energy ratio is not affected.

3.1.3. Influence of decreased porosity on the strength and fracture energy

The Young's modulus was determined non-destructively using IET before the samples were notched for the fracture energy measurement in order to ensure a proper analysis. The modulus increased with every infiltration step, starting with 50.8 GPa at 40.0 % porosity until it reached a maximum of 77.8 GPa at a porosity of 34.3 % (Fig. 5).

With decreasing porosity and increasing Young's modulus, the measurement of the fracture energy became more difficult since the elastic energy stored in the testing setup as well as in the sample increased, resulting in a less stable crack growth. In samples with a

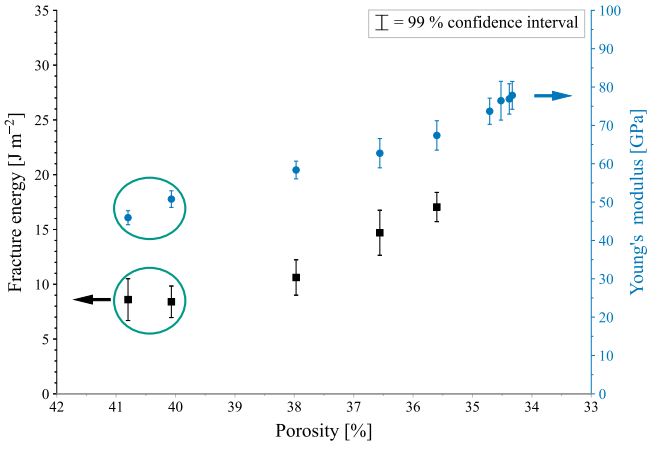

Fig. 5. Fracture energy and Young's modulus as a function of decreasing porosity. The heat treatments have no significant effect on the fracture energy but lead to a discernible increase of the Young's modulus (circled samples). The error bars show the confidence interval for 99 % with a sample size of 30 for each group for Young's modulus and at least 17 samples for each fracture energy measurement.

porosity of 35.6 %–40.0 % (0–3 infiltrations), at least a semi-stable behavior was always achieved. Fig. 6 shows exemplary force-displacement curves for heat-treated samples as well as samples after one to three infiltrations.

The fracture behavior changed from nearly stable crack growth at 40.0 % porosity (heat-treated) to a barely semi-stable crack growth after three infiltrations and a porosity of 35.6 %. After four infiltrations and below a porosity of 34.7 %, catastrophic crack growth occurred for all samples. Therefore, the calculation of the fracture energy was no longer possible, since less energy than stored in the system (sample + testing machine) might be necessary for complete crack growth. The loss of the needed semi-stable fracture behavior identifies the boundaries of the method. If the matrix fracture energy is too high, it becomes more difficult to perform a valid test. While it is possible to obtain a fracture energy calculating the K_{IC} from the peak load and afterwards transforming it into a fracture energy, the calculations have an error of 30 % which must be taken into account when evaluating the data [21]. For this study, only values obtained from the work-of-fracture approach were used to guarantee the full comparability between all stages of infiltration. Consequently, only samples, which were infiltrated up to three times, were used for fracture energy measurements. The change in porosity between a heat-treated sample and a sample after three infiltrations can be seen clearly in the SEM images in Fig. 7 as well.

With every infiltration step, the fracture energy increased (Fig. 5), starting at around 8.4 J/m^2 at a porosity of 40.0 % until a maximum of 17.1 J/m^2 at 35.6 % porosity was reached. The fracture toughness changed from 0.53 MPa•m$^{0.5}$–0.95 MPa•m$^{0.5}$, which is comparable to the change of partially sintered TM-DAR and CT-2000 SG, which both had a fracture toughness of around 0.5 MPa•m$^{0.5}$ at a porosity of 40 % and around 1.1 MPa•m$^{0.5}$ at a porosity of 30 % [37]. Table 1 provides all determined data together with the calculated ratio used as fracture energy ratio and elastic mismatch.

The decrease of fracture energy with increasing porosity is in accordance with other measurements for ceramic materials [42]. For porosities of under 20 % in alumina, the influence seems to be negligible, but with a higher amount of pore volume, the fracture energy starts to decrease. The pore size seems to have no influence as long as it is small compared to the tested volume [40,43].

3.2. Theoretical influence of porosity on the properties of a composite

In the study of He and Hutchinson [4], the behavior of a crack at an interface between two materials was described. In our previous work, we reported a loss of the damage-tolerant behavior at a submicron matrix porosity of 34 % [26]. The present work focused on the determination of the fracture energy of a matrix used in an Ox/Ox material with good damage-tolerant behavior, using the work-of-fracture approach. Therefore, the fracture energy of samples with different porosities was measured and compared with the crack deflection criterion. To incorporate our data into the model developed by He and Hutchinson, a reference value for the fracture energy of dense alumina fibers was used. Alumina fibers have a small grain size, resulting in excellent mechanical properties. Therefore, a reference value can be obtained of small grained alumina. The grains affect the fracture energy, but below 25 μm, the influence for alumina seems to be negligible and the fracture energy has been reported with around 20 J/m^2 [30,38–40], which is in agreement with the fracture energy of most ceramic fibers [7]. Therefore, the reference value for the fracture energy of the Nextel™ 610

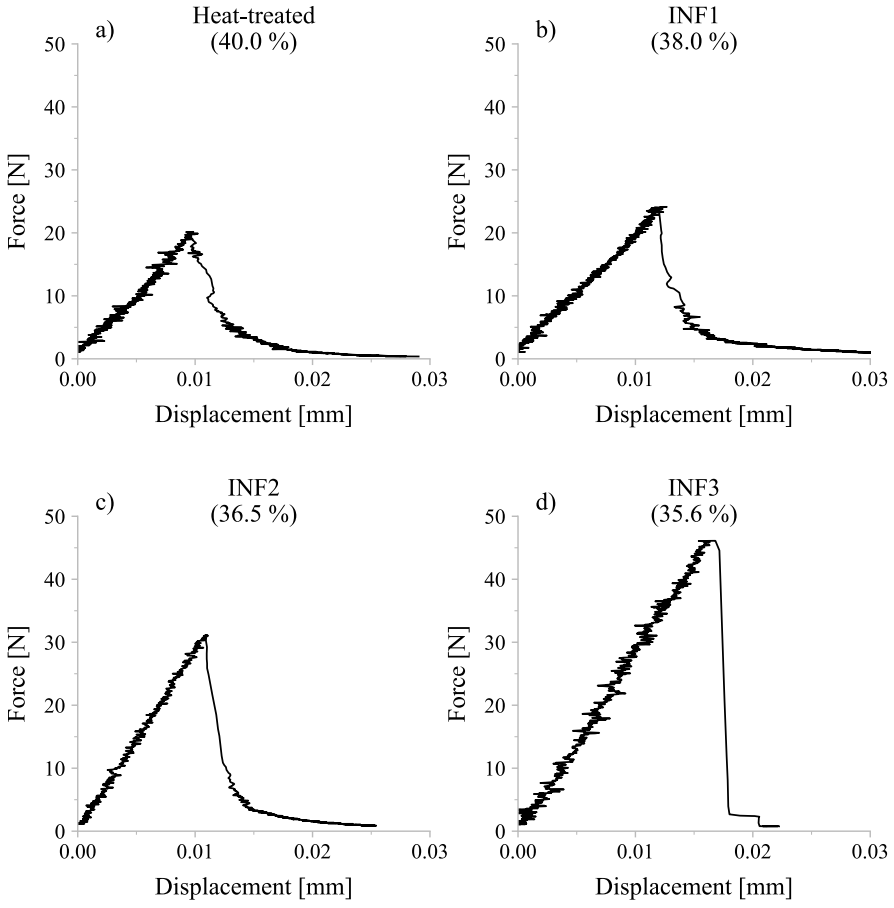

Fig. 6. Force-displacement curves for heat-treated as well as for infiltrated samples. The semi-stable crack growth behavior can be seen clearly for heat-treated samples (a)) as well as for one or two infiltrations (b) & c)). After three infiltrations however, the semi-stable behavior is less pronounced (d)).

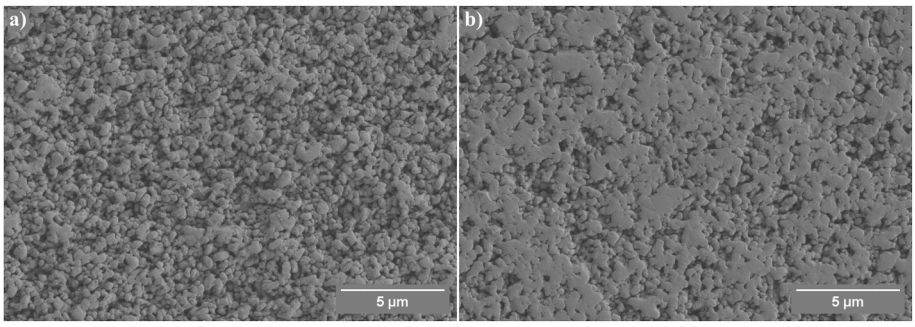

Fig. 7. SEM images (SE-mode) of a a) heat-treated sample. b) sample after three infiltrations. The loss of porosity due to precursor infiltration is clearly visible.

Table 1
Results of porosity, Young's modulus, fracture toughness and fracture energy measurements together with the calculated ratios for the classification ($\Gamma_f = 20$ J/m^2 [7, 38–40]; $E_f = 370$ GPa [41]). The sample count in brackets is the number of samples produced and corresponds to the samples tested for porosity and Young's modulus. The numbers without brackets indicate the amount of valid tested samples for fracture toughness and fracture energy.

ID	Sample count	Porosity [%]	Young's modulus E_m [GPa]	Fracture toughness K_{1c} [MPa•m$^{0.5}$]	Fracture energy Γ_i [J/m^2]	Ratio Γ_i/Γ_f	Elastic mismatch $(E_f-E_m)/(E_f+E_m)$
as-fired	22 (30)	40.8 ± 0.8	46.9 ± 4.1	0.54 ± 0.10	8.6 ± 3.6	0.43	0.78
heat-treated	26 (30)	40.0 ± 1.4	50.8 ± 4.8	0.53 ± 0.09	8.4 ± 3.0	0.42	0.76
INF1	25 (30)	38.0 ± 0.6	58.4 ± 5.1	0.71 ± 0.13	10.6 ± 3.3	0.53	0.73
INF2	26 (30)	36.5 ± 1.0	62.8 ± 8.5	0.87 ± 0.17	14.7 ± 4.2	0.73	0.71
INF3	17 (30)	35.6 ± 0.7	67.4 ± 8.6	0.95 ± 0.13	17.1 ± 2.1	0.85	0.69
INF4	0 (30)	34.7 ± 0.5	73.7 ± 7.6	–	–	–	–
INF5	0 (30)	34.5 ± 0.6	76.4 ± 11.3	–	–	–	–
INF6	0 (30)	34.4 ± 0.7	76.9 ± 8.8	–	–	–	–
INF7	0 (30)	34.3 ± 0.9	77.8 ± 8.1	–	–	–	–

alumina fibers was set to 20 J/m^2. This follows the procedure described by Shimoda et al. [10], where the fracture energy of a dense sample was also set as the fracture energy of the fibers of the same material. To calculate the ratio of the Young's moduli, 370 GPa was used as the value of the fibers according to the manufacturer [41].

With increasing fracture energy of the matrix, the fracture energy ratio of the material approaches the theoretical boundary conditions between crack deflection and crack propagation (solid black line, Fig. 8). For Ox/Ox with the Al_2O_3-ZrO_2-matrix investigated in the present study, the loss of damage-tolerant behavior is predicted for porosities between 35.6 % and 36.5 %, which corresponds to a change of the elastic mismatch from 0.71 to 0.69 and a change in the fracture energy ratio from 0.73 to 0.85. The prediction is in excellent agreement with the results of our previous study [26], where we observed a loss of damage-tolerant behavior for an Ox/Ox in the matrix porosity range of 34 %–37 % [26]. The results of the work-of-fracture method matches the findings in our Ox/Ox material very well. Therefore, a precise prediction of the behavior for a new matrix material is expected. The inability to examine even denser samples is not a disadvantage for the prediction in this study, since the change from crack deflection to crack penetration was covered.

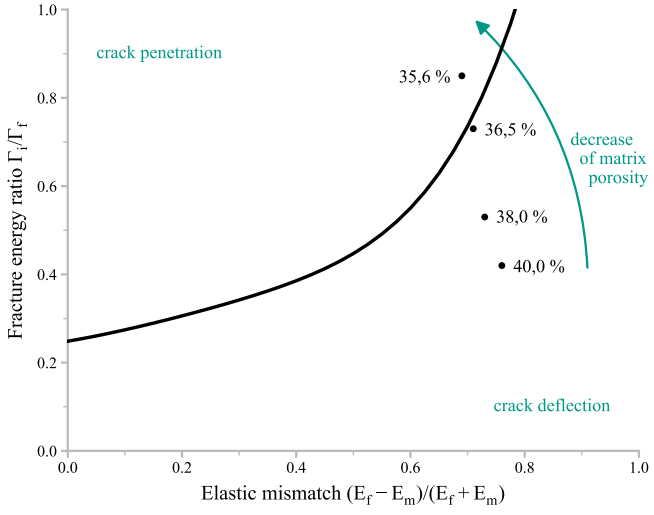

Fig. 8. The fracture energy ratio increased with decreasing porosity, crossing the line between crack deflection and crack propagation. According to the model of He and Hutchinson, crack deflection is expected below the solid line and therefore at 36.5 % porosity and above, but crack penetration will occur at 35.6 % porosity or less, resulting in a predicted change from damage-tolerant behavior to brittle failure for a WMC. This is in good agreement with our previous work, where an Ox/Ox material with the same matrix material as tested in this study, lost its damage-tolerant behavior between 37 % and 34 % matrix porosity [26].

The increasing fracture energy ratio with decreasing porosity was already described for the development of a porous WMC-SiC/SiC [10]. At 20 % porosity, a brittle failure was found, while a damage-tolerant behavior started to occur at 30 % porosity. The same trend was also observed for heat treated Ox/Ox [1,12]. In the mentioned studies, a system of alumina fibers and a mullite or mullite-alumina matrix was heat treated at 1200 °C for 2 h, 100 h and 1000 h. The elastic mismatch decreased due to the thermal aging, while the fracture energy ratio increased. However, the thermal aging did not lead to a change from crack deflection to crack penetration. Accordingly, the Ox/Ox material on which the studies were based on showed no change of the damage-tolerant behavior following similar heat treatments [19], although only one sample had the same composition and treatment as the monolithic material. However, a direct comparison between monolithic and fiber reinforced materials was not made. Our study therefore extends the predictions for a WMC with an alumina-zirconia matrix system and Nextel™ 610 fibers and additionally provides the direct comparison with an Ox/Ox material treated the exact same way as the monolithic samples used in this study. Furthermore, a particularly easy way of determining the suitability of a matrix material for any

given fiber type was presented. The composition or manufacturing method of the tested material system has no influence on the individual results, since all values needed for the predictions can be obtained by the same set of samples. Keeping in mind, that the development of new material is possible without such reinfiltration cycles, the encountered possible porosity gradient as well as the loss of a (semi-) stable fracture behavior for porosities lower than 35.6 % are deemed to be of minor importance for the development of a WMC. The method enables an assessment of the matrix properties without the usually variable-dependent production of a CMC. Omitting the fibers also results in a significant reduction in development costs, since unsuitable materials can be discarded before the use of expensive fibers. The predictions can be validated by subsequently manufacturing and testing the novel materials based on the weak matrix concept for CMC. Since both the monolithic sample in this study as well as the Ox/Ox of our previous study were densified by a liquid polymer infiltration and pyrolysis process, there are no constraints during densification. For different systems, which show a higher matrix shrinkage, the possibility of constrained sintering due to the non-shrinking fibers has to be considered. The development of a new material based on this study is in progress and the experiments will be submitted for publication in the near future.

4. Conclusion

A simple method for the classification of a potential matrix material for a weak matrix composite (WMC) in the model of He and Hutchinson was investigated. The determination of the fracture energy was based on the work-of-fracture approach. The matrix of an all-oxide ceramic matrix composite (Ox/Ox) investigated in a prior study was used as a model system. Thus, a direct comparison of the theoretical predictions of the method based on monolithic samples with the findings gained from an existing Ox/Ox was possible. In this regard, the influence of a decreasing porosity on the fracture energy of an alumina-zirconia system was investigated. The stable or semi-stable crack growth needed to calculate the fracture energy could be obtained for samples with a porosity of 35.6 % and above. The decreasing porosity caused an increase in the Young's modulus and fracture energy, starting at 50.8 GPa and 8.4 J/m^2 for 40.0 % porosity. A maximum was reached at 35.6 % porosity with a modulus of 67.4 GPa and a fracture energy of 17.1 J/m^2. Hence the model of He and Hutchinson [4] predicted a damage-tolerant behavior for a alumina fiber-based Ox/Ox with a matrix porosity of 36.5 % and a fracture energy of 14.7 J/m^2, but a brittle behavior with 35.6 % porosity and a fracture energy of 17.1 J/m^2. This was in agreement with our previous work, where the damage-tolerant behavior was lost between 34 % and 37 % submicron matrix porosity [26].

Due to the direct measurement of the fracture energy and the Young's Modulus of a potential matrix material, the method allows a general assessment of a possible crack deflection. As a result, different systems can be compared without the need for expensive fibers, which saves resources as well as costs in the development of weak matrix composites.

CRediT authorship contribution statement

Lukas Wagner: Writing – review & editing, Writing – original draft, Visualization, Validation, Methodology, Investigation, Formal analysis, Data curation, Conceptualization. **Georg Puchas:** Writing – review & editing, Visualization, Validation, Supervision, Resources, Project administration, Methodology, Investigation, Funding acquisition, Formal analysis, Data curation, Conceptualization. **Stefan Flauder:** Writing – review & editing, Validation, Methodology, Formal analysis, Data curation. **Bernd Martin:** Writing – review & editing, Methodology, Conceptualization. **Stefan Schafföner:** Writing – review & editing, Validation, Supervision, Resources, Project administration, Funding acquisition, Conceptualization.

Funding

This work was funded by the Deutsche Forschungsgemeinschaft (DFG) under grant agreement 518255159 (FlexFiber).

Declaration of competing interest

The authors declare that they have no known competing financial interests or personal relationships that could have appeared to influence the work reported in this paper.

References

[1] F.W. Zok, Developments in oxide fiber composites, J. Am. Ceram. Soc. 89 (2006) 3309–3324, https://doi.org/10.1111/j.1551-2916.2006.01342.x.
[2] F.W. Zok, C.G. Levi, Mechanical properties of porous-matrix ceramic composites, Adv. Eng. Mater. 3 (2001) 15–23, https://doi.org/10.1002/1527-2648(200101)3:1/2<15::AID-ADEM15>3.0.CO;2-A.
[3] C.G. Levi, J.Y. Yang, B.J. Dalgleish, F.W. Zok, A.G. Evans, Processing and performance of an all-oxide ceramic composite, J. Am. Ceram. Soc. 81 (2005) 2077–2086, https://doi.org/10.1111/j.1151-2916.1998.tb02590.x.
[4] M.-Y. He, J.W. Hutchinson, Crack deflection at an interface between dissimilar elastic materials, Int. J. Solid Struct. 25 (1989) 1053–1067, https://doi.org/10.1016/0020-7683(89)90021-8.
[5] A.G. Evans, D.B. Marshall, Overview no. 85 the mechanical behavior of ceramic matrix composites, Acta Metall. 37 (1989) 2567–2583, https://doi.org/10.1016/0001-6160(89)90291-5.
[6] W.-C. Tu, F.F. Lange, A.G. Evans, Concept for a damage-tolerant ceramic composite with "strong" interfaces, J. Am. Ceram. Soc. 79 (1996) 417–424, https://doi.org/10.1111/j.1151-2916.1996.tb08138.x.
[7] A.G. Evans, F.W. Zok, The physics and mechanics of fibre-reinforced brittle matrix composites, J. Mater. Sci. 29 (1994) 3857–3896, https://doi.org/10.1007/BF00355946.
[8] K.A. Keller, G. Jefferson, R.J. Kerans, Oxide-oxide composites, Ceram. Matrix Compos. (2014) 236–272, https://doi.org/10.1002/9781118832998.ch8. Hoboken, NJ, USA: John Wiley & Sons, Inc.
[9] R.M.G. De Meyere, K. Song, L. Gale, S. Harris, I.M. Edmonds, T.J. Marrow, et al., A novel trench fibre push-out method to evaluate interfacial failure in long fibre composites, J. Mater. Res. 36 (2021) 2305–2314, https://doi.org/10.1557/s43578-021-00153-1.
[10] K. Shimoda, T. Hinoki, Y.-H. Park, Development of non-brittle fracture in SiCf/SiC composites without a fiber/matrix interface due to the porous structure of the matrix, Compos. Part A Appl. Sci. Manuf 115 (2018) 397–404, https://doi.org/10.1016/j.compositesa.2018.10.005.
[11] X. Chen, X. Lv, H. Liu, R. Jiang, X. Sun, Effect of matrix microstructure on micro- and macro-mechanical properties of 2.5D woven oxide fiber reinforced oxide matrix composites, Compos. Commun. 52 (2024) 102159, https://doi.org/10.1016/j.coco.2024.102159.
[12] H. Fujita, G. Jefferson, R.M. McMeeking, F.W. Zok, Mullite/alumina mixtures for use as porous matrices in oxide fiber composites, J. Am. Ceram. Soc. 87 (2004) 261–267, https://doi.org/10.1111/j.1551-2916.2004.00261.x.
[13] P.O. Guglielmi, D. Blaese, M.P. Hablitzel, G.F. Nunes, V.R. Lauth, D. Hotza, et al., Microstructure and flexural properties of multilayered fiber-reinforced oxide composites fabricated by a novel lamination route, Ceram. Int. 41 (2015) 7836–7846, https://doi.org/10.1016/j.ceramint.2015.02.120.
[14] R.W. Davidge, G. Tappin, The effective surface energy of brittle materials, J. Mater. Sci. 3 (1968) 165–173, https://doi.org/10.1007/BF00585484.
[15] Y.X. Wang, Q.H. Shang, Y.Q. Liu, D.H. Zhang, Fracture energy of mullite ceramic heat storage material under thermal shock conditions, Mater. Res. Innov. 19 (2015), https://doi.org/10.1179/1432891715Z.0000000002001. S9-318-S9-321.
[16] L.J. Malvar, G.E. Warren, Fracture energy for three-point-bend tests on single-edge-notched beams, Exp. Mech. 28 (1988) 266–272, https://doi.org/10.1007/BF02329022.
[17] J. Nakayama, Direct measurement of fracture energies of brittle heterogeneous materials, J. Am. Ceram. Soc. 48 (1965) 583–587, https://doi.org/10.1111/j.1151-2916.1965.tb14677.x.
[18] H. Fujita, C.G. Levi, F.W. Zok, G. Jefferson, Controlling mechanical properties of porous mullite/alumina mixtures via precursor-derived alumina, J. Am. Ceram. Soc. 88 (2005) 367–375, https://doi.org/10.1111/j.1551-2916.2005.00061.x.
[19] H. Fujita, Development and Assessment of Two-phase Porous Matrices for Use in All-Oxide Ceramic Composites, University of California, Santa Barbara, 2004.
[20] E.A.V. Carelli, H. Fujita, J.Y. Yang, F.W. Zok, Effects of thermal aging on the mechanical properties of a porous-matrix ceramic composite, J. Am. Ceram. Soc. 85 (2002) 595–602, https://doi.org/10.1111/j.1151-2916.2002.tb00138.x.
[21] H. Fujita, C.G. Levi, F.W. Zok, G. Jefferson, Controlling mechanical properties of porous mullite/alumina mixtures via precursor-derived alumina, J. Am. Ceram. Soc. 88 (2005) 367–375, https://doi.org/10.1111/j.1551-2916.2005.00061.x.
[22] G. Puchas, S. Möckel, W. Krenkel, Novel prepreg manufacturing process for oxide fiber composites, J. Eur. Ceram. Soc. 40 (2020) 5930–5941, https://doi.org/10.1016/j.jeurceramsoc.2020.06.064.

[23] F. Lindner, G. Puchas, S. Schafföner, Novel measuring method for prepreg processability of oxide fiber ceramic matrix composites, Compos Part A Appl Sci Manuf 162 (2022) 107131, https://doi.org/10.1016/j.compositesa.2022.107131.
[24] J. Winkelbauer, G. Puchas, W. Krenkel, S. Schafföner, Short fiber spraying process of all-oxide ceramic matrix composites: a parameter study, Int. J. Appl. Ceram. Technol. 20 (2023) 754–767, https://doi.org/10.1111/ijac.14196.
[25] J. Winkelbauer, G. Puchas, S. Schafföner, W. Krenkel, Short fiber-reinforced oxide fiber composites, Int. J. Appl. Ceram. Technol. 19 (2022) 1136–1147, https://doi.org/10.1111/ijac.13931.
[26] L. Wagner, G. Puchas, W. Krenkel, S. Schafföner, Influence of matrix densification on the properties of weak matrix oxide fiber composites, Compos Part A Appl Sci Manuf 164 (2023) 107274, https://doi.org/10.1016/j.compositesa.2022.107274.
[27] H. Liu, R. Jiang, X. Sun, X. Chen, G. Deng, Microstructure and mechanical properties of Al2O3/Al2O3 composite densified through a slurry infiltration and sintering process, J. Mater. Res. Technol. 25 (2023) 2925–2935, https://doi.org/10.1016/j.jmrt.2023.06.167.
[28] F. Yang, Y. Jiang, R. Jiang, H. Liu, Y. Zhang, X. Sun, Microstructure, mechanical properties and thermal stability of Al2O3/Al2O3 ceramic matrix composites obtained from submicron-sized powers, Ceram. Int. 50 (2024) 9710–9720, https://doi.org/10.1016/j.ceramint.2023.12.289.
[29] X. Sun, Z. Tian, R. Jiang, H. Liu, Slurry infiltration and sintering cycle-dependent mechanical properties of 3D oxide/oxide ceramic matrix composites, Int. J. Appl. Ceram. Technol. 21 (2024) 655–663, https://doi.org/10.1111/ijac.14592.
[30] K.K. Chawla, C. Coffin, Z.R. Xu, Interface engineering in oxide fibre/oxide matrix composites, Int. Mater. Rev. 45 (2000) 165–189, https://doi.org/10.1179/095066000101528359.
[31] J. Helbig, Wet Processing of Nanosized Ceramic Particles, ETH Zurich, 2000, https://doi.org/10.3929/ethz-a-003876189.
[32] T. Wamser, S. Scheler, B. Martin, W. Krenkel, Novel oxide fiber composites by freeze casting, J. Eur. Ceram. Soc. 34 (2014) 3827–3833, https://doi.org/10.1016/j.jeurceramsoc.2014.06.015.
[33] M.A. Mattoni, J.Y. Yang, C.G. Levi, F.W. Zok, Effects of matrix porosity on the mechanical properties of a porous-matrix, all-oxide ceramic composite, J. Am. Ceram. Soc. 84 (2001) 2594–2602, https://doi.org/10.1111/j.1151-2916.2001.tb01059.x.
[34] F. Zok, F.F. Lange, J.R. Porter, Packing density of composite powder mixtures, J. Am. Ceram. Soc. 74 (1991) 1880–1885, https://doi.org/10.1111/j.1151-2916.1991.tb07803.x.
[35] G.V. Guinea, J. Planas, M. Elices, Measurement of the fracture energy using three-point bend tests: Part 1—influence of experimental procedures, Mater. Struct. 25 (1992) 212–218, https://doi.org/10.1007/BF02473065.
[36] A.T. Zehnder, Fracture Mechanics, Springer Science+Business Media, London ; New York, 2012.
[37] T. Ostrowski, J. Rödel, Evolution of mechanical properties of porous alumina during free sintering and hot pressing, J. Am. Ceram. Soc. 82 (1999) 3080–3086, https://doi.org/10.1111/j.1151-2916.1999.tb02206.x.
[38] R.W. Rice, S.W. Freiman, P.F. Becher, Grain-size dependence of fracture energy in ceramics: I, experiment, J. Am. Ceram. Soc. 64 (1981) 345–350, https://doi.org/10.1111/j.1151-2916.1981.tb10300.x.
[39] R.W. Rice, S.W. Freiman, Grain-size dependence of fracture energy in ceramics: II, A model for noncubic materials, J. Am. Ceram. Soc. 64 (1981) 350–354, https://doi.org/10.1111/j.1151-2916.1981.tb10301.x.
[40] J. Wang, L.J. Vandeperre, W.J. Clegg, Effect of Grain Size on the Fracture Behaviour of Porous Alumina Made by Partial Sintering of Powder Compacts, 2008, pp. 233–241, https://doi.org/10.1002/9780470294703.ch29.
[41] 3M Advanced Materials Division, 3M Nextel Ceramic Fibers and Textiles, Technical Reference Guide, 2021.
[42] R.W. Rice, Grain size and porosity dependence of ceramic fracture energy and toughness at 22 °C, J. Mater. Sci. 31 (1996) 1969–1983, https://doi.org/10.1007/BF00356616.
[43] L.J. Vandeperre, J. Wang, W.J. Clegg, Effects of porosity on the measured fracture energy of brittle materials, Philos. Mag. 84 (2004) 3689–3704, https://doi.org/10.1080/14786430412331293522.